SUPPLEMENTARY INFORMATION: NMRlipids III: Lipid-cholesterol interactions in atomistic resolution molecular dynamics simulations

Fernando Favela-Rosales,[†] Peter Heftberger,[‡] Matti Javanainen,[¶] Jesper J. Madsen,[‖] Josef Melcr,[#] Markus Miettinen,[@] O. H. Samuli Ollila,[*,#] Georg Pabst,[‡] and Thomas Piggot[▽]

†*Departamento de Física, Centro de Investigación y de Estudios Avanzados del IPN, Apartado Postal 14-740, 07000 México D.F., México*

‡*University of Graz*

¶*Department of Physics, Tampere University of Technology, Tampere, Finland*

§*University of Helsinki*

‖*Department of Global Health, College of Public Health*

⊥*University of South Florida*

#*Institute of Organic Chemistry and Biochemistry, Academy of Sciences of the Czech Republic, Prague 6, Czech Republic*

@*MPI*

△*Institute of Biotechnology, University of Helsinki*

▽*University of Southampton*

E-mail: samuli.ollila@helsinki.fi

S1 Simulation Parameters

The force field specific simulation parameters used for each force field are listed in Table **??**. The parameter input files (`.mdp`) are provided in the Zenodo portal (links in the main text).

For all simulations, we used an integration time step of 2 fs and the leap-frog integrator of GROMACS. The isothermal–isobarit (NPT) ensemble was used with a temperature of 298 K and a pressure of 1 bar. All simulations were 1 µs long, and trajectories were written every 1 ns. The P-LINCS constraint algorithm[1,2] was used for the bonds noted in Table **??**.

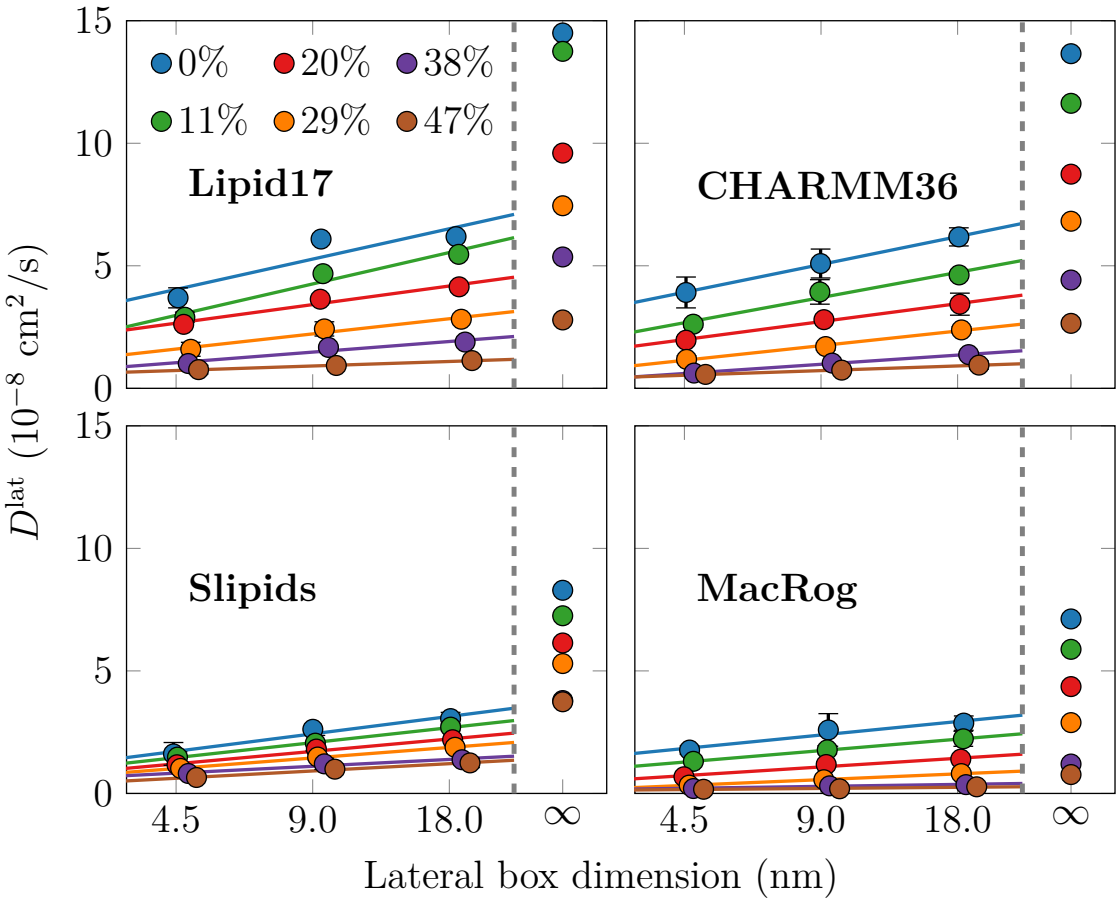

Figure S1: **Dependence of lateral diffusion coefficients on simulation box size.** The values calculated for the lipid centres of mass with `gmx msd` after eliminating leaflet drift. The values for the three system sizes are shown as markers together with fits of Eq. (**??**). The values extrapolated to infinite system sizes are also shown in the separate column.

Table S1: Simulation parameters used for different force fields.

Parameter	**CHARMM36**	**Slipids**	**Lipid17**	**MacRog**
Neighbour list type	Verlet[3]	Verlet[3]	Verlet[3]	Verlet[3]
Long-range electrostatics	PME	PME	PME	PME
LJ cut-off	1.2 nm	1.4 nm	0.9 nm	1.0 nm
LJ modifier	Force switch 1.0–1.2 nm	–	–	–
Dispersion correction	–	Energy & pressure[4]	Energy & pressure[4]	Energy & pressure[4]
Thermostat	Nosé–Hoover[5,6]	Stochastic rescaling[7]	Nosé–Hoover[5,6]	Stochastic rescaling[7]
Time constant (T)	1 ps	0.5 ps	1 ps	0.1 ps
Coupling groups	Lipids & water	Lipids & water	Lipids & water	Lipids & water
Barostat	Parrinello–Rahman[8]	Berendsen[9]	Parrinello–Rahman[8]	Parrinello–Rahman[8]
Coupling type (P)	semi-isotropic	semi-isotropic	semi-isotropic	semi-isotropic
Time constant (P)	5 ps	10 ps	5 ps	4 ps
Compressibility	$4.5{\cdot}10^{-5}$ 1/bar	$4.5{\cdot}10^{-5}$ 1/bar	$4.5{\cdot}10^{-5}$ 1/bar	$4.5{\cdot}10^{-5}$ 1/bar
Constraints	Bonds with H	All bonds	Bonds with H	All bonds
Water model	TIPS3P[10]	TIP3P[11]	TIP3P[11]	TIP3P[11]
FF Source	CHARMM-GUI	CHARMM-GUI	CHARMM-GUI	Refs. 12 & 13
Parameter source	CHARMM-GUI	Slipids website	CHARMM-GUI	Refs. 12 & 13

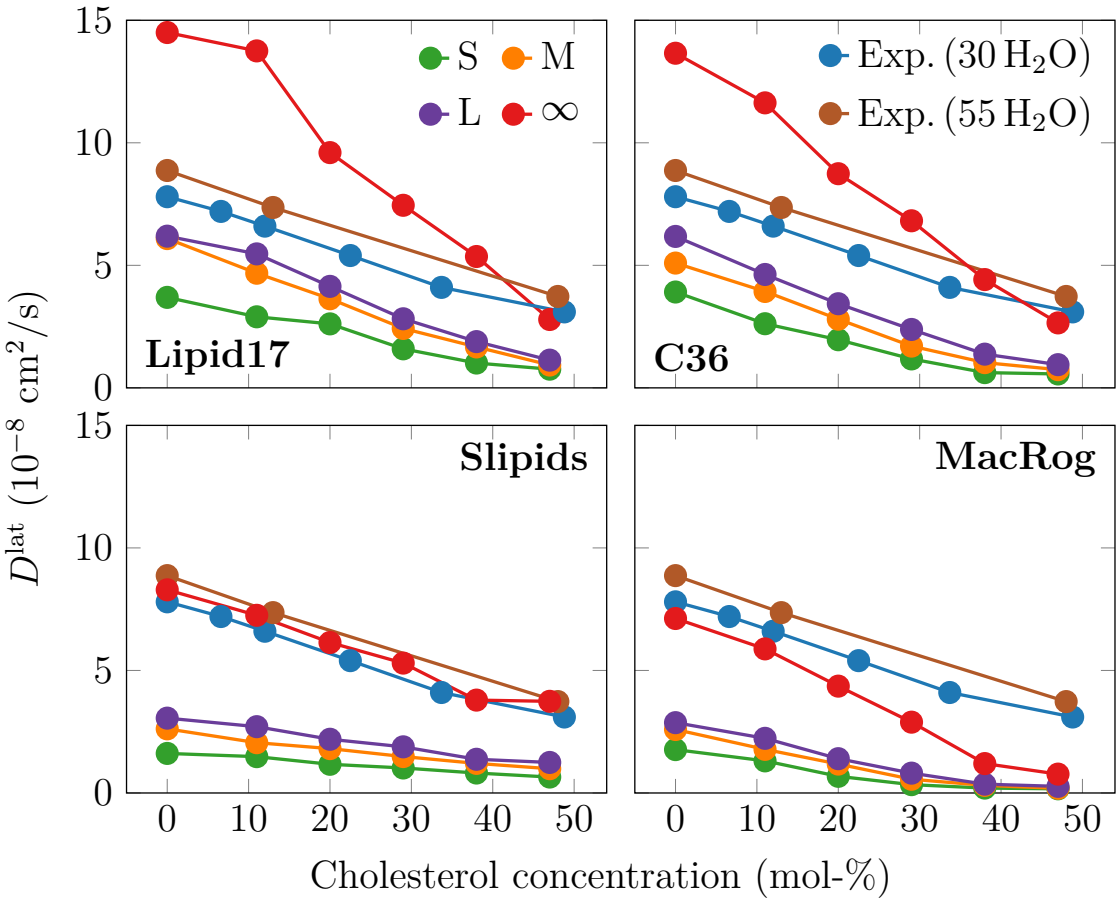

Figure S2: **Dependence of lateral diffusion coefficients on cholesterol concentration.** Data are shown for all system sizes; small (S), medium (M), and large (L). The values extrapolated to infinity are shown as well (∞). Experimental measured at two hydration levels, 30 m-% and 55-% of water.[14,15]

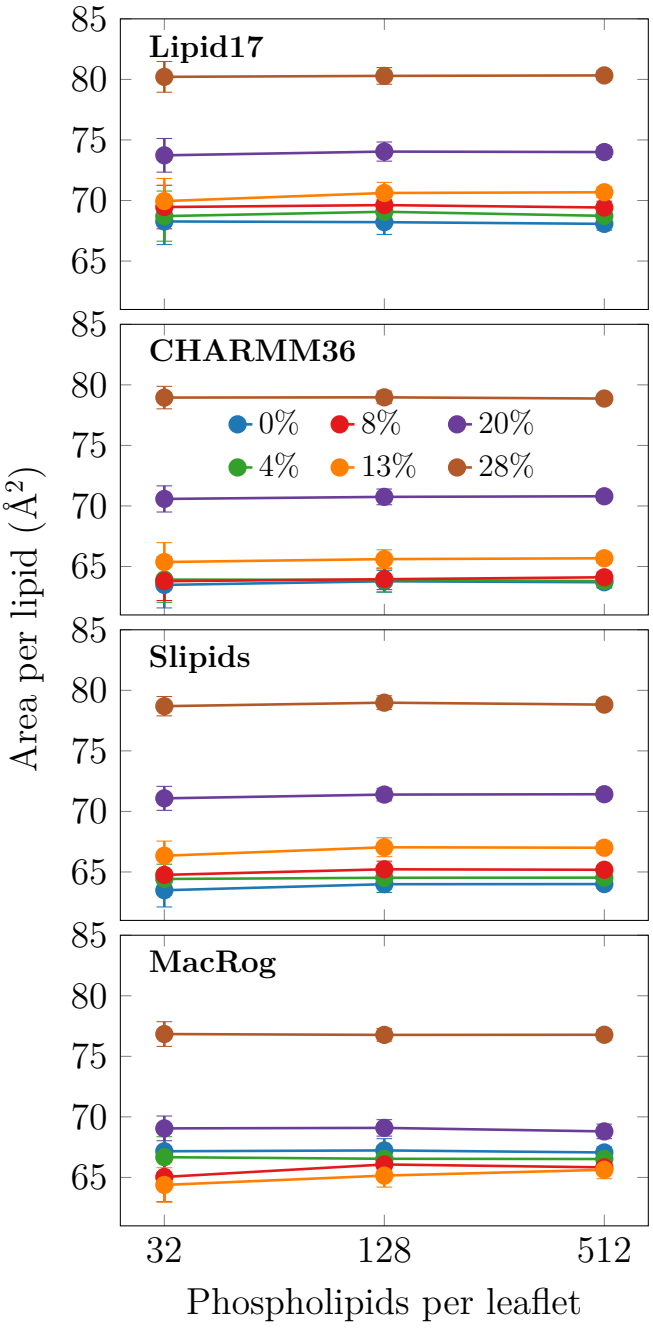

Figure S3: **Dependence of area per lipid on simulation box size.** Area per lipid is calculated by dividing the membrane area by the number of lipids in one leaflet. Error bars show standard error extracted using block averaging in `gmx analyze`.

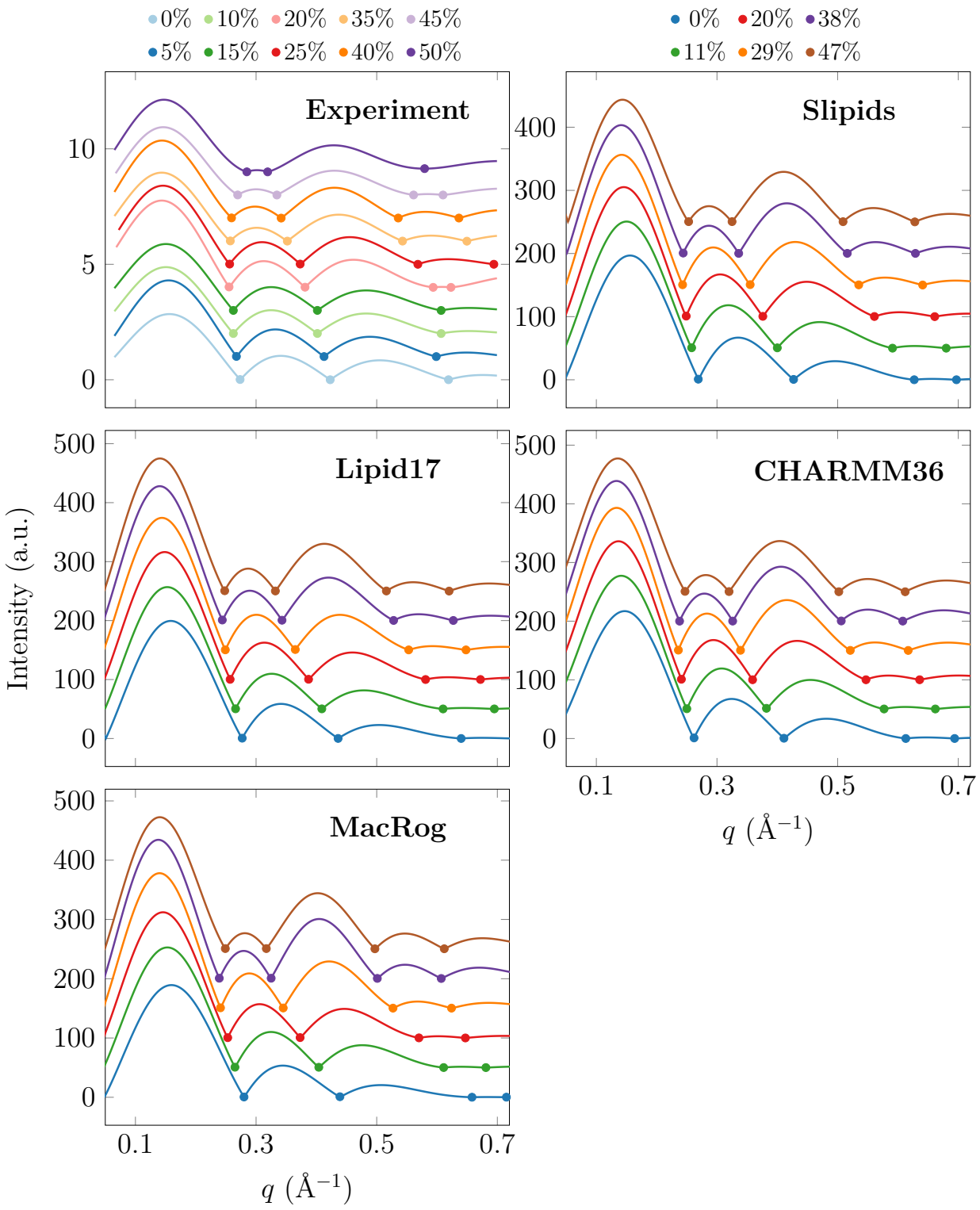

Figure S4: **Scattering intensities as a function of scattering vector from experiments and simulations.** Each of the profiles is shifted vertically with respect to the previous one, by 1 for the experimental profiles and by 50 for the computational ones. The minima are marked by filled circles to guide the eye.

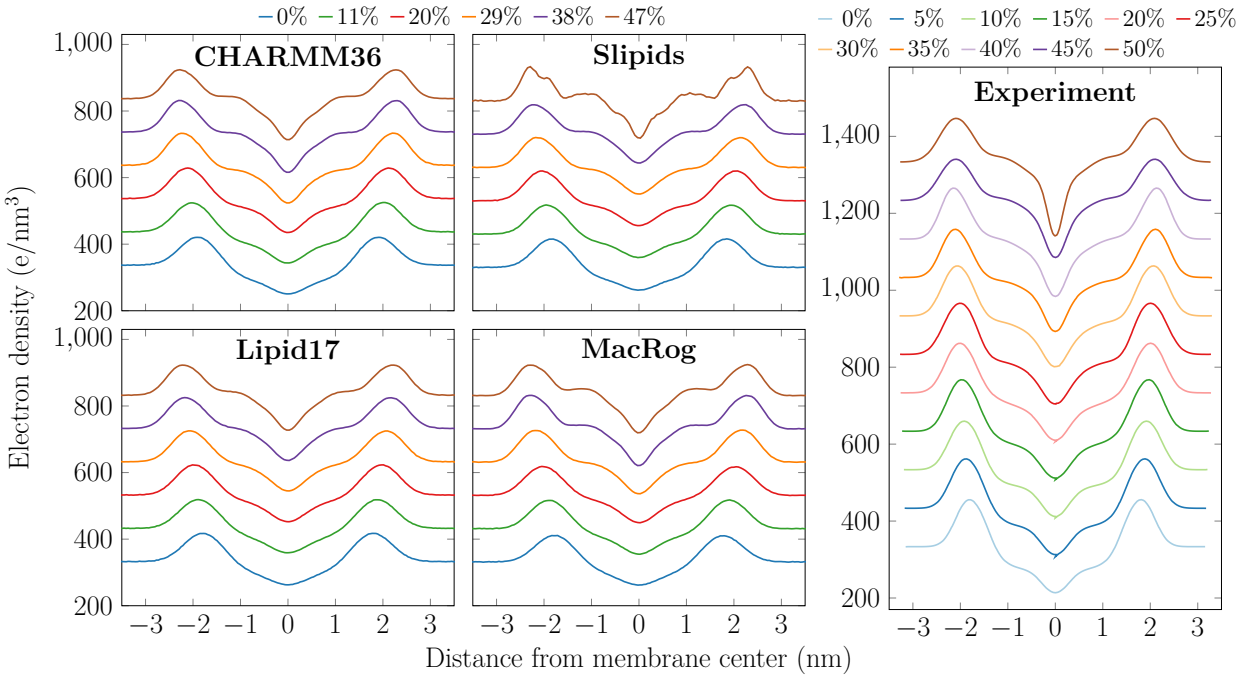

Figure S5: **Electron density profiles.** Each of the profiles is shifted vertically with respect to the previous one by 100 units.

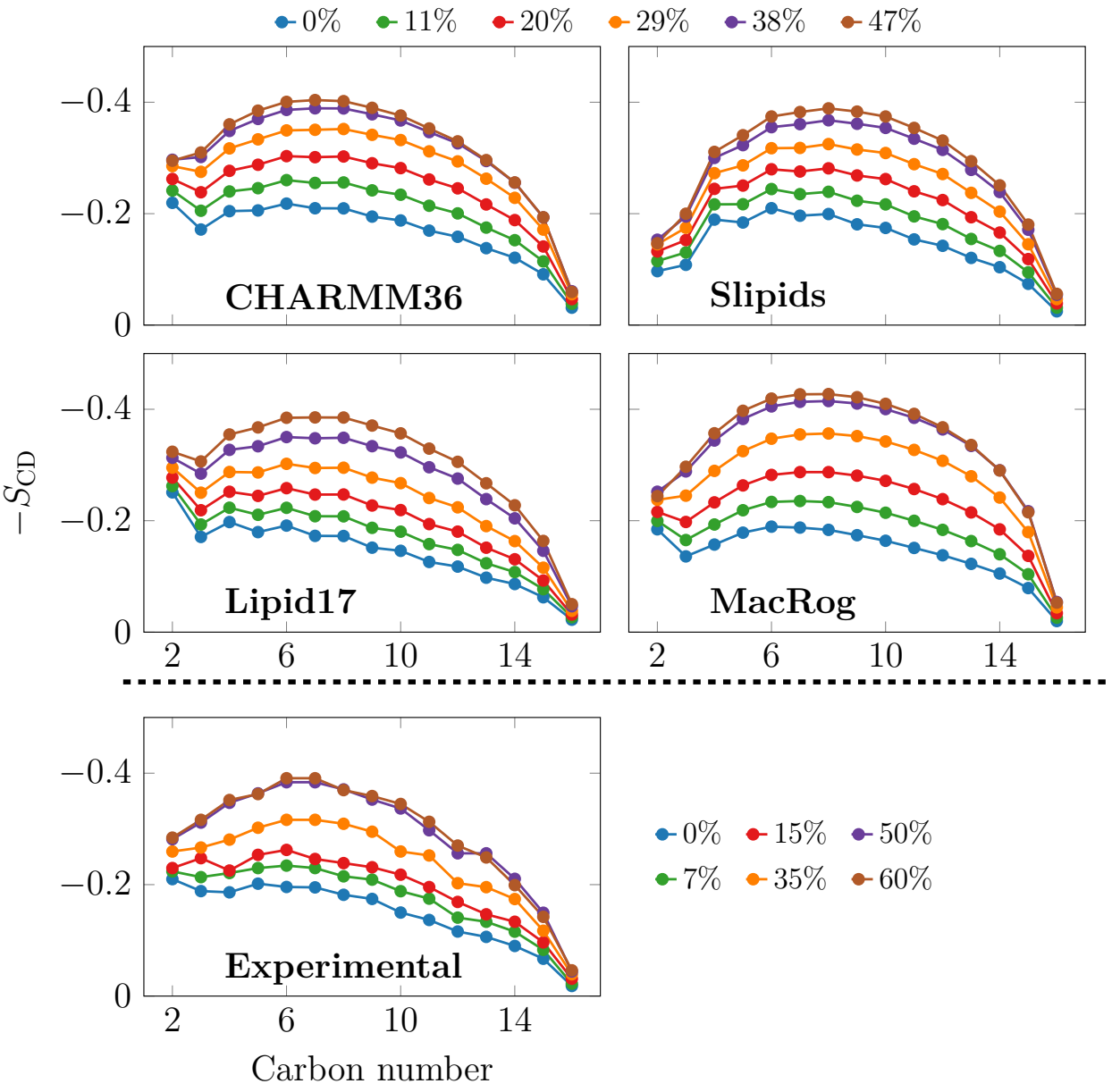

Figure S6: **Effect of cholesterol on the acyl chain order parameters of the POPC *sn*-1 (palmitate) chain.** The legend at the top corresponds to all simulations, and the one at the bottom to the experiments.

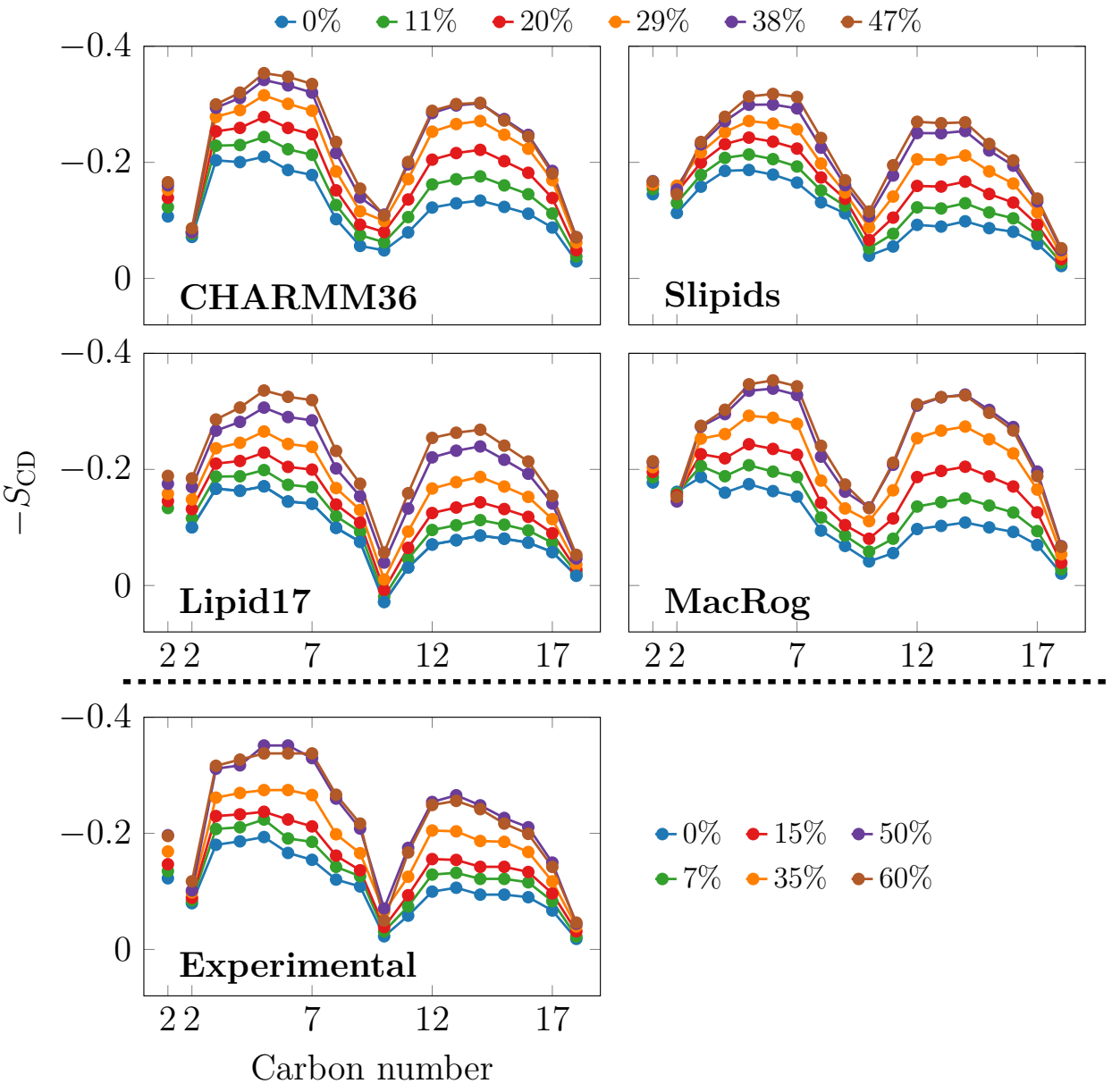

Figure S7: **Effect of cholesterol on the acyl chain order parameters of the POPC *sn*-2 (oleate) chain.** The legend at the top corresponds to all simulations, and the one at the bottom to the experiments. Since the order parameters measured for the two hydrogens bound to the C2 carbon differ, they are both shown in the plots.

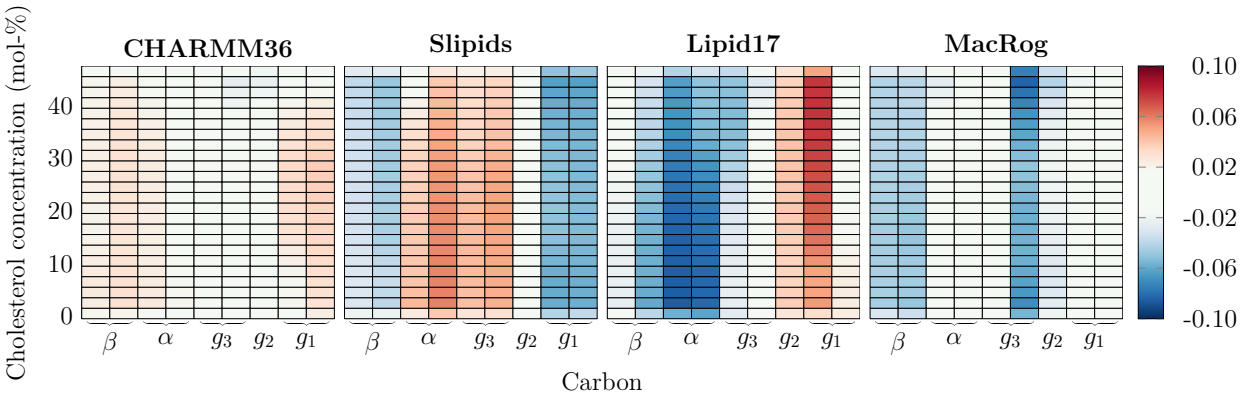

Figure S8: **The deviation of POPC head group parameters from experimental values as a function of CHOL concentration.**

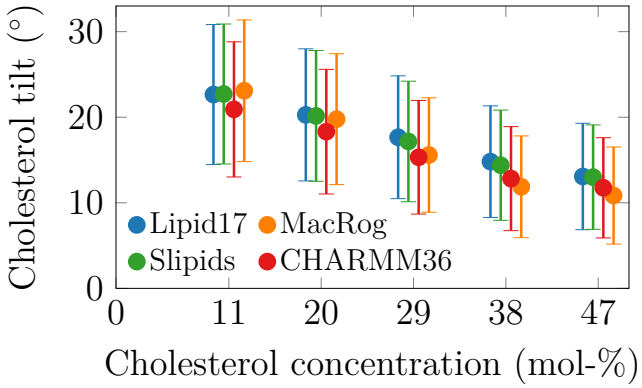

Figure S9: **Effect of cholesterol concentration on the tilt of the cholesterol molecules.** The tilt is defined as the angle between the vector connecting the C3 and C17 carbons at the two ends of the rigid ring structure of cholesterol. The hydroxyl group is bound to C3 and the hydrocarbon chain to C17. The tilt distributions were gathered from the two leaflets, fitted with a Gamma distribution, and the mean values and standard deviations were extracted and shown here as the value and error estimate, respectively. The cholesterol concentration was identical between the simulations, but the points are horizontally slightly shifted for clarity.

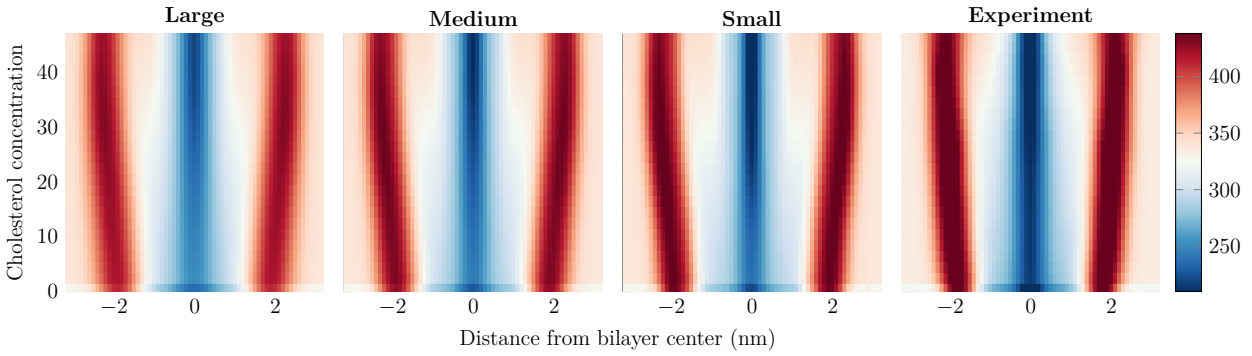

Figure S10: **Effect of system size on the density profiles.** Membrane undulations are larger in the larger systems, which leads to the smearing of the electron density profiles. Here, data are shown for CHARMM36 in the large (1024 POPC in total), medium (256 POPC in total), or small (64 POPC in total) systems. The experimental electron density profile is shown for comparison.

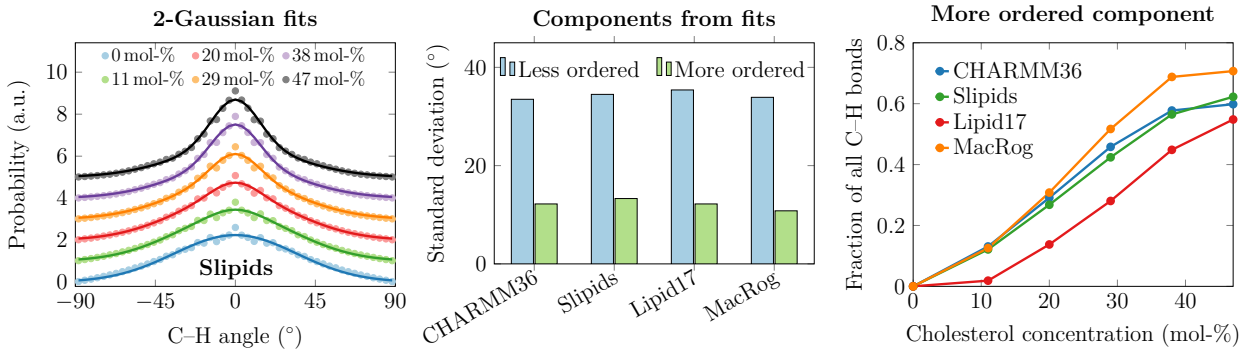

Figure S11: **Distributions of C–H bond orientations.** Leftmost panel: The probability distributions for the angle of C–H vectors of the last 6 carbons in the palmitate chain of POPC with respect to the xy-plane. All distributions are centered around 0, but have different shapes. The markers show data extracted from Slipids simulations at various CHOL concentrations, and the solid lines show two-Gaussian fits with fixed standard deviations to the data. These Gaussians correspond to the more and less ordered palmitate chains. The fixed standard deviations were extracted from a fit of two Gaussians to the data accumulated across all CHOL concentrations. The fit with the fixed standard deviations to all CHOL concentrations are excellent with $R^2 = 0.991 \pm 0.005$ (mean±standard deviation). Middle panel: The standard deviations of the two Gaussians fitted to the C–H distribution (such as the one in the leftmost panel) for the four force fields. Rightmost panel: The fraction of the more ordered component as a function of CHOL concentration extracted simply by dividing the prefactor in the Gaussian distribution for the more ordered component by the sum of the two prefactors. Notably, in the CHOL-free system, the ordered component is not present.

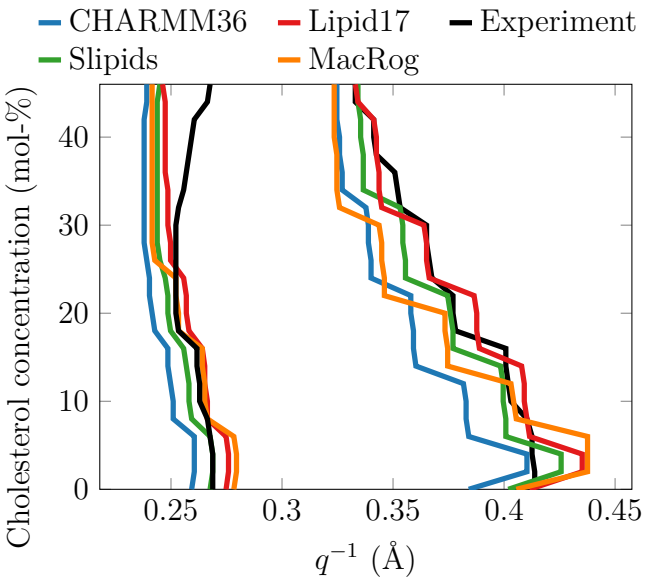

Figure S12: **Effecf of CHOL on the location of the first two minima in the form factor.** The minima are extracted from the form factors interpolated to all CHOL concentrations (Fig. S4) from experiment and simulation with the `findpeaks` function in Matlab.

References

(1) Hess, B.; Bekker, H.; Berendsen, H. J. C.; Fraaije, J. G. E. M. LINCS: a linear constraint solver for molecular dynamics simulations. *J. Comput. Chem.* **1997**, *18*, 1463–1472.

(2) Hess, B. P-LINCS: A Parallel Linear Constraint Solver for Molecular Simulation. *J. Chem. Theory Comput.* **2008**, *4*, 116–122.

(3) Páll, S.; Hess, B. A flexible algorithm for calculating pair interactions on SIMD architectures. *Computer Physics Communications* **2013**, *184*, 2641–2650.

(4) Shirts, M. R.; Mobley, D. L.; Chodera, J. D.; Pande, V. S. Accurate and efficient corrections for missing dispersion interactions in molecular simulations. *The journal of physical chemistry B* **2007**, *111*, 13052–13063.

(5) Hoover, W. G. Canonical dynamics: Equilibrium phase-space distributions. *Phys. Rev. A* **1985**, *31*, 1695–1697.

(6) Nose, S. A molecular dynamics method for simulations in the canonical ensemble. *Mol. Phys.* **1984**, *52*, 255–268.

(7) Bussi, G.; Donadio, D.; Parrinello, M. Canonical sampling through velocity rescaling. *J. Chem. Phys.* **2007**, *126*.

(8) Parrinello, M.; Rahman, A. Polymorphic transitions in single crystals: A new molecular dynamics method. *Journal of Applied physics* **1981**, *52*, 7182–7190.

(9) Berendsen, H. J.; Postma, J. v.; Van Gunsteren, W. F.; DiNola, A.; Haak, J. R. Molecular dynamics with coupling to an external bath. *The Journal of chemical physics* **1984**, *81*, 3684–3690.

(10) Durell, S. R.; Brooks, B. R.; Ben-Naim, A. Solvent-induced forces between two hydrophilic groups. *The Journal of Physical Chemistry* **1994**, *98*, 2198–2202.

(11) Jorgensen, W. L.; Chandrasekhar, J.; Madura, J. D.; Impey, R. W.; Klein, M. L. Comparison of simple potential functions for simulating liquid water. *J. Chem. Phys.* **1983**, *79*, 926–935.

(12) Kulig, W.; Pasenkiewicz-Gierula, M.; Róg, T. Cis and trans unsaturated phosphatidylcholine bilayers: a molecular dynamics simulation study. *Chemistry and physics of lipids* **2016**, *195*, 12–20.

(13) Milan Rodriguez, P.; Fuchs, P. F. MacRog pure POPC MD simulation (300 K - 500ns - 1 bar). 2020; `https://doi.org/10.5281/zenodo.3741793`.

(14) Filippov, A.; Orädd, G.; Lindblom, G. The effect of cholesterol on the lateral diffusion of phospholipids in oriented bilayers. *Biophysical journal* **2003**, *84*, 3079–3086.

(15) Filippov, A.; Orädd, G.; Lindblom, G. Influence of cholesterol and water content on phospholipid lateral diffusion in bilayers. *Langmuir* **2003**, *19*, 6397–6400.